

## Optical Bistability under Nonresonant Excitation in Spinor Polariton Condensates

L. Pickup,<sup>1</sup> K. Kalinin,<sup>2</sup> A. Askitopoulos,<sup>1</sup> Z. Hatzopoulos,<sup>3,4</sup> P. G. Savvidis,<sup>3,5,6</sup> N. G. Berloff,<sup>2,7</sup> and P. G. Lagoudakis<sup>1,2</sup>

<sup>1</sup>*School of Physics and Astronomy, University of Southampton, Southampton SO17 1BJ, United Kingdom*

<sup>2</sup>*Skolkovo Institute of Science and Technology, Moscow 143026, Russian Federation*

<sup>3</sup>*Microelectronics Research Group, IESL-FORTH, P.O. Box 1527, 71110 Heraklion, Crete, Greece*

<sup>4</sup>*Department of Physics, University of Crete, 71003 Heraklion, Crete, Greece*

<sup>5</sup>*Department of Materials Science and Technology, University of Crete, 71003, Crete, Greece*

<sup>6</sup>*ITMO University, St. Petersburg 197101, Russia*

<sup>7</sup>*Department of Applied Mathematics and Theoretical Physics, University of Cambridge, Cambridge CB3 0WA, United Kingdom*



(Received 22 September 2017; revised manuscript received 5 February 2018; published 30 May 2018)

We realize bistability in the spinor of polariton condensates under nonresonant optical excitation and in the absence of biasing external fields. Numerical modeling of the system using the Ginzburg-Landau equation with an internal Josephson coupling between the two spin components of the condensate qualitatively describes the experimental observations. We demonstrate that polariton spin bistability strongly depends on the condensate's overlap with the exciton reservoir by tuning the excitation geometry and sample temperature. We obtain noncollapsing bistability hysteresis loops for a record range of sweep times, [10  $\mu$ s, 1 s], offering a promising route to spin switches and spin memory elements.

DOI: [10.1103/PhysRevLett.120.225301](https://doi.org/10.1103/PhysRevLett.120.225301)

Optical bistability is the phenomenon of an optical system supporting two or more stable states for a given range of driving conditions [1,2]. A bistable behavior demonstrates an internal memory of the system, which could potentially be harnessed to form optical transistors and memory elements. It has been observed in systems such as cold atoms [3], lasers [4], self-electro-optic effect devices [5], and Fabry-Pérot cavities containing nonlinear materials [6,7]. Optical bistability in microcavity polaritons, the bosonic quasiparticles formed by the strong coupling of cavity photons and excitons, was previously demonstrated for resonant or quiresonant optical excitation [8–13], electrical biasing [14,15], and nonresonant electrical injection [16]. In resonantly pumped microcavity polaritons, bistability was described by a Kerr-like nonlinearity resulting from polariton-polariton interactions [9] and by employing an analogy with optical parametric oscillators [10]. Under electrical injection, bistability was observed in the photoluminescence intensity, in the presence of an external magnetic field, and was attributed to the electrostatic screening of the injected charge carriers forming a positive feedback for the backward sweep of the driving current [16].

Bistability has also been realized in the spinor of a polariton state utilizing the polaritons' well-defined spin and its one-to-one correspondence with the circular polarization of emitted light. Optical control of polariton spin was employed in the realization of spin bistability and multistability, using quiresonant optical excitation of a cylindrical mesa [8] by rotating the polarization of the optical pump. Recently, spin bistability was also shown under

nonresonant optical excitation in a mesa-structured microcavity using a biasing electrical field to induce an energy splitting between two linear polarization modes while keeping the optical excitation constant [14]. Under nonresonant pumping and in the absence of external fields, the preferable route for the operation of all-optical memory elements in polariton circuits, both polariton bistability and spin bistability remain elusive, despite theoretical predictions [17].

For the observation of polariton bistability or spin bistability, it is essential that the population fluctuations of polaritons or the relative spin populations remain sufficiently small so as not to bridge the two stable solutions of the system that would lead to a collapse of the hysteresis loop. Polaritons are an inherently open-dissipative, nonequilibrium system that requires continuous pumping to reach the steady state due to a finite cavity lifetime. In the absence of external electric or magnetic fields, polariton bistability and spin bistability have been observed only under resonant excitation; the fundamental difference between resonant and nonresonant optical pumping is the presence, in the latter case, of a hot-exciton reservoir and the concomitant exciton-polariton interactions. Exciton-polariton pair scattering events contribute to the decoherence of polaritons [18,19]; however, the observed bistabilities in polariton systems occur at time-scales that can exceed the coherence time of a polariton condensate by a factor of  $10^9$ , suggesting that it is not the exciton-induced decoherence that precludes the observation of bistability under nonresonant pumping. Another source of instability that prevents bistable behavior under

nonresonant pumping is the density fluctuations induced by the hot-exciton reservoir. Similarly, exciton-polariton interactions are a strong source of spin mixing [20] that, in the presence of an initial spin imbalance, result in changes of the relative spin populations that prevent the realization of spinor polariton bistability.

In this Letter, we realize spin bistability under nonresonant optical pumping, in the absence of external fields, by spatially separating the spin-bistable polariton state from the hot-exciton reservoir, thus strongly suppressing spin depolarization in the system. The spin bistability is evidenced on the spinor of a polariton condensate, trapped at the center of an annular excitation beam, in the form of a hysteresis loop in the degree of circular polarization versus the optical excitation power. We attribute the spin bistability to an interplay of polariton nonlinearities with the internal Josephson coupling of the two spin components. Figure 1 depicts a schematic of the system; the red ring on the surface of the microcavity shows the pumping intensity profile. The rainbow-colored Gaussian, in the center of the ring, shows the measured polariton density of the ground state,  $\psi_{00}$ . The black mesh annular barrier represents the repulsive potential due to the optically injected hot-exciton reservoir. The red and blue spheres in the center of the ring represent the two spin components of the polariton condensate that are coupled via an internal Josephson coupling  $J$ .

The microcavity we use in this study is a  $5\lambda/2$  cavity with GaAs quantum wells (QWs), as in Ref. [21], held at  $\sim 6$  K using a continuous flow cold finger cryostat. We excite the sample with a linearly polarized, continuous wave (cw), monomode laser, tuned to the first reflectivity minimum at 754 nm. A spatial light modulator (SLM) imprints a phase profile, and the desired annular pump

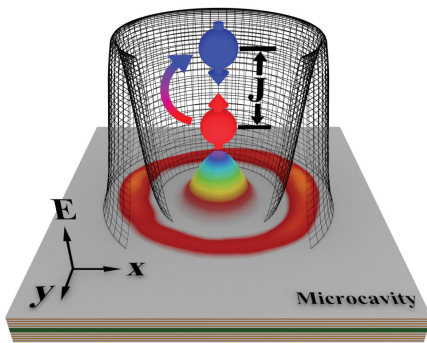


FIG. 1. Schematic of the optical excitation scheme. The red ring on the surface of the microcavity is an intensity map of the pump beam; the black mesh annular barrier represents the confining potential due to the exciton reservoir. A section of the barrier is removed to show the trapped condensate shown as the rainbow-colored Gaussian mode in the center of the confining potential. The red and the blue spheres show the spin-up and spin-down states forming the condensate, respectively. The arrow shows a current of polaritons between the two spin states.

geometry is focused on the sample surface by a 0.4 numerical aperture (NA) microscope objective lens. The intensity of the laser is modulated into triangular pulses using an acousto-optical modulator (AOM) that is driven by a triangular voltage pulse train. A polarization analyzer is used to record the two cross-circular components of the photoluminescence intensity. The top schematic in Fig. 2 shows the setup and the triangular laser pulse train used to excite the sample. The use of a high NA excitation lens in

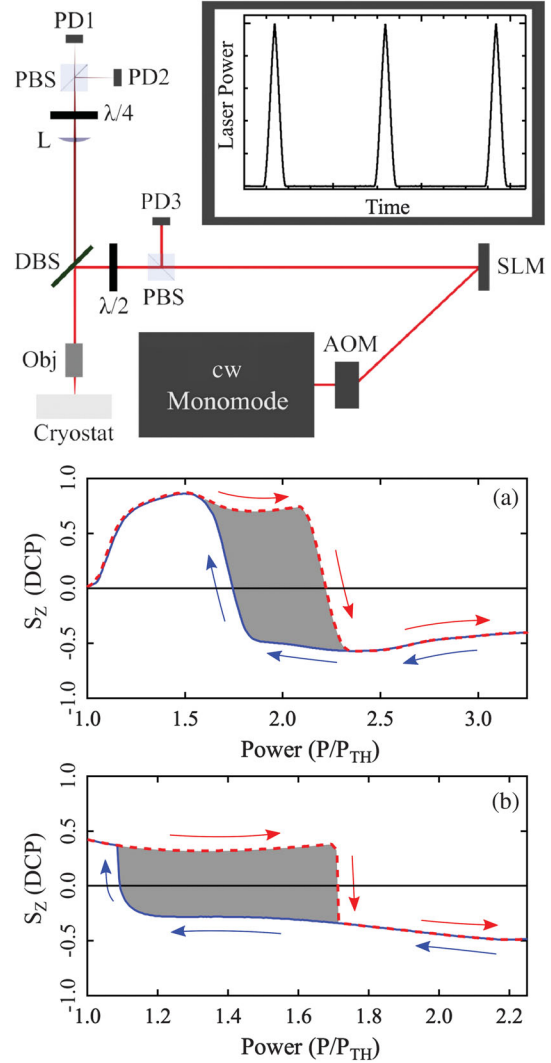


FIG. 2. Schematic of the experimental setup. SLM, spatial light modulator; AOM, acousto-optical modulator; PBS, polarizing beam splitter; DBS, dichroic beam splitter; Obj, microscope objective lens;  $L$ , plano-convex lens;  $\lambda/4$ , quarter wave plate;  $\lambda/2$ , half wave plate; and PD (1,2,3) photodiodes measuring the spin components of the photoluminescence and the corresponding laser intensity. (a) Measured third Stokes component  $S_Z$ , representing the degree of circular polarization (DCP) versus pump power displaying the characteristic hysteresis loop of bistability for an annulus of  $\sim 16.1 \mu\text{m}$  diameter and 1.67 ms sweep time at a detuning of  $-7.6$  meV. (b) Hysteresis loop in  $S_Z$  versus pump power resulting from the numerical simulations.

combination with the samples birefringence introduces a  $\sim 10\%$  ellipticity to the pump beam [22], which creates a small spin imbalance in the injected carriers. Since the electron spin relaxation time in GaAs QWs is longer than the carrier relaxation time to the exciton reservoir, the initial electron spin imbalance is reflected in the spin imbalance of the exciton reservoir that, in turn, leads to a spin-polarized polariton condensate [23]; by separating the polariton condensate from the exciton reservoir here, we observe 93% degree of circular polarization (DCP).

Figure 2(a) shows a typical hysteresis loop in the DCP, represented by the  $S_z$  component of the Stokes polarization vector versus the pump power normalized to the condensation threshold at a detuning of  $-7.6$  meV. With an increasing pump power, shown with a red dashed line in Fig. 2(a), we observe a spin reversal, as was previously observed in time-integrated measurements [23]. The spin reversal was attributed to the transition into a desynchronization regime in Ref. [23] through the complex spin-dependent Ginzburg-Landau equations with an internal Josephson coupling term between the two spinor components. With a decreasing pump power (blue solid line), a backwards spin reversal is observed at a lower pumping power compared to the power for the spin reversal observed in the forward direction. The signature of spin bistability is qualitatively reproduced numerically with the same theoretical model of Ref. [23] as shown in Fig. 2(b); see Appendix A of Supplemental Material [24].

To gain an understanding of the nature of polariton spin bistability, in the following we draw analogues with the driven damped pendulum. We nondimensionalize the complex spin-dependent Ginzburg-Landau equation and the rate equation describing the density in the exciton reservoir and reduce them to the equation of a driven-damped pendulum:

$$\ddot{\Theta} + \beta(p)\dot{\Theta} = -I_{\text{bias}}(p) - I_{\text{cr}}(p) \sin \Theta, \quad (1)$$

where  $\Theta$  is the phase difference between two spin components,  $\beta$  is a damping coefficient (positive above the threshold) that increases with the pumping power approaching a value of  $1/2$ ,  $I_{\text{bias}}$  is equivalent to the driving torque of a pendulum, and  $I_{\text{cr}}$  is equivalent to the maximum gravitational torque. A description of the process of nondimensionalization and reduction is presented in Appendix A of Supplemental Material [24].

A driven damped pendulum supports two types of solution [25]: If the torques' ratio  $I = |I_{\text{bias}}|/|I_{\text{cr}}| \leq 1$ , then the pendulum's trajectory is attracted to a fixed point (stationary solutions regime), where the angular displacement is constant ( $\dot{\Theta} = 0$ ) for a fixed driving torque. Alternatively, if  $I > 1$ , then  $\dot{\Theta} \neq 0$ , in which case the pendulum continues to overturn even under a fixed driving torque (limit cycle solutions regime). In this scheme, bistability occurs in the backward ramp of the driving

torque due to its inertia, where the backward ramp corresponds to a decreasing pump power.

Here, the stationary solutions regime results in the phases of the two spin states evolving synchronously with a constant phase difference; see the top branch of the bistability in Figs. 2(a) and 2(b). The limit cycle solutions regime,  $\dot{\Theta} \neq 0$ , results in the desynchronized evolution of the spin states' phases. With a decreasing pump power, the role of the "inertia" increases due to the decrease of the damping rate  $\beta$ , which allows for the limit cycle solutions regime to persist for pump powers lower than those on the forward ramp, leading to the observed hysteresis. A schematic comparison between bistability in the driven damped pendulum and the spinor polariton condensate is presented in Appendix B of Supplemental Material [24].

In the following, we investigate the dependence of the observed bistability on the overlap,  $\Omega$ , between the condensate and the hot-exciton reservoir. At low temperatures, the pump-induced exciton reservoir is colocalized with the pump beam due to the small (submicron) exciton diffusion length, which allows us to control  $\Omega$  by changing the diameter of the annular pump profile. For diameters ranging from  $11.8$  to  $17.9$   $\mu\text{m}$ , polariton condensation occurs in a Gaussian-shaped ground state  $\psi_{00}$ . Figure 3(a) shows the dependence of the hysteresis area on the diameter of the annular pump at a detuning of  $-7.6$  meV (black diamonds). With an increasing pump diameter from  $11.8$  to  $17.9$   $\mu\text{m}$ , the hysteresis area increases monotonically. The (red) dotted line in Fig. 3(a) shows the calculated  $\Omega$  assuming a Gaussian-shaped condensate and an annular pump profile with a Gaussian cross section, where the width of the condensate and the annular profile are approximated from the measured photoluminescence under different annular pump diameters. When the diameter of the annular pump exceeds  $18$   $\mu\text{m}$ , the trapping potential allows for the coexistence of higher-order Hermite-Gaussian-shaped,  $\psi_{01}$ , condensates with the  $\psi_{00}$  condensate [26]; this leads to the collapse of the hysteresis loop. The hysteresis loops versus the diameter of the annular pump are presented in Appendix C of Supplemental Material [24]. The deleterious effect of exciton-polariton interactions on bistability is further corroborated by changing the exciton fraction of polaritons. The solid black circle in Fig. 3(a) shows the hysteresis area obtained for an annular pump diameter of  $13.1$   $\mu\text{m}$  at a detuning of  $-11.2$  meV.

Figure 3(b) shows the hysteresis area versus temperature ranging from  $4$  to  $40$  K, where strong coupling is sustained [27]. With an increasing temperature, the exciton linewidth, the exciton reservoir lifetime, the exciton diffusion length, and the exciton-photon detuning are increasing. All of these effects contribute in the suppression of the hysteresis area. We note that the observed hysteresis loops under all previous excitation and detuning conditions disappear when we switch from monomode (low-intensity fluctuations) to multimode cw excitation lasers; the latter induce

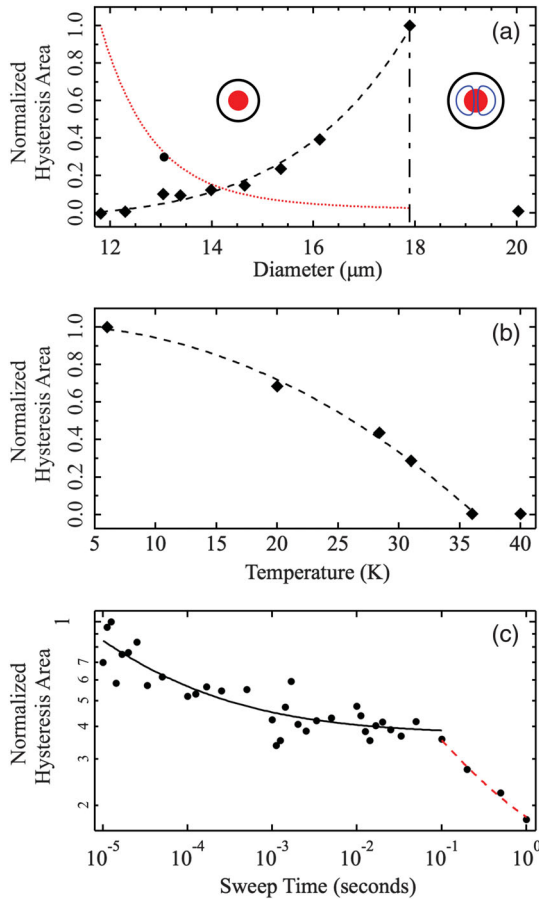


FIG. 3. (a) The dependence of the hysteresis area (symbols) on the diameter of the annular pump at  $\sim 6$  K. The dotted red line shows the estimated overlap between the condensate and exciton reservoir,  $\Omega$ , versus the annular pump diameter. The vertical dash-dotted line separates the regimes wherein only the ground state  $\psi_{00}$ , or both  $\psi_{00}$  and the first excited state  $\psi_{01}$ , coexists. (b) Temperature dependence of the hysteresis area for an  $\sim 15.4$   $\mu\text{m}$  diameter annular pump. The data in (a) and (b) are recorded with a 1 ms sweep time. (c) Hysteresis area as a function of sweep time  $T_p$  for an  $\sim 13.1$   $\mu\text{m}$  diameter annular pump recorded at  $\sim 6$  K. The black (red) lines are power-law fits. In all of the above data points, solid circles are recorded at a detuning of  $-11.2$  meV, while solid diamonds at  $-7.6$  meV.

density fluctuations in the exciton reservoir that are mirrored in the density of the condensate leading to the collapse of bistability [28].

Relevant to the applications in volatile memories and switching is the range of sweep times wherein the bistable behavior is durable, i.e., noncollapsing hysteresis loops. To that end, we investigate the relationship of the hysteresis area on the duration of the sweep time ( $T_p$ ). Figure 3(c) shows the hysteresis area for sweep times spanning 5 orders of magnitude  $T_p \in [10 \mu\text{s}, 1 \text{s}]$ , where bistability is observed in the absence of collapses [29]. We observe that the dependence of the hysteresis area as a function of the sweep time exhibits a double power-law decay. The mean-field approach of the spin-dependent Ginzburg-Landau

model implemented here to explain the observed bistability cannot reproduce the dependence of the hysteresis area on the sweep time. Recently, a double power-law decay versus the sweep time was attributed to quantum fluctuations [30]. An evolution from a double to a single power-law decay was experimentally observed with increasing the average photon number and was ascribed to a dissipative phase transition between the quantum regime and the thermodynamic limit [13]. The dissipative phase transition was shown to depend strongly on the laser-cavity detuning; here spinor bistability is observed under nonresonant optical pumping.

In summary, we demonstrate optical bistability in spinor polariton condensates under nonresonant optical excitation in the absence of external biasing fields. The hysteresis loop can be qualitatively modeled through the complex spin-dependent Ginzburg-Landau equations with an internal Josephson coupling term between the two spinor components. We unravel the detrimental role of a hot-exciton reservoir on bistability by controlling the overlap of the pump-induced exciton reservoir and the polariton condensate. The dependence of spin bistability on the condensate's overlap with the exciton reservoir allows us to control the hysteresis area by tuning the excitation geometry. Most importantly, we obtain noncollapsing bistability hysteresis loops for a record range of sweep times,  $[10 \mu\text{s}, 1 \text{s}]$ , offering a promising route to spin switches and spin memory elements.

This work was carried out in the framework of the joint Russian-Greek project ‘Polisimulator’ supported by the Ministry of Education and Science of The Russian Federation (Project No. RFMEFI61617X0085), Greece and the EU Regional Development Fund and the United Kingdom’s Engineering and Physical Sciences Research Council (Grant No. EP/M025330/1 on hybrid polaritonics). The authors would like to acknowledge valuable discussions with J. D. Töpfer.

- [1] E. Abraham and S. D. Smith, Optical bistability and related devices, *Rep. Prog. Phys.* **45**, 815 (1982).
- [2] H. Gibbs, *Optical Bistability: Controlling Light with Light* (Elsevier, New York, 2012).
- [3] A. Joshi, A. Brown, H. Wang, and M. Xiao, Controlling optical bistability in a three-level atomic system, *Phys. Rev. A* **67**, 041801 (2003).
- [4] P. Jung, G. Gray, R. Roy, and P. Mandel, Scaling Law for Dynamical Hysteresis, *Phys. Rev. Lett.* **65**, 1873 (1990).
- [5] F. Forsmann, D. Jäger, and W. Niessen, Nonresonant optical bistability in InP:Fe seed devices, *Opt. Commun.* **62**, 193 (1987).
- [6] P. W. Smith and E. H. Turner, A bistable Fabry-Perot resonator, *Appl. Phys. Lett.* **30**, 280 (1977).
- [7] H. M. Gibbs, S. L. McCall, and T. N. C. Venkatesan, Differential Gain and Bistability Using a Sodium-Filled Fabry-Perot Interferometer, *Phys. Rev. Lett.* **36**, 1135 (1976).

- [8] T. K. Paraíso, M. Wouters, Y. Léger, F. Morier-Genoud, and B. Deveaud-Plédran, Multistability of a coherent spin ensemble in a semiconductor microcavity, *Nat. Mater.* **9**, 655 (2010).
- [9] A. Baas, J. Ph. Karr, H. Eleuch, and E. Giacobino, Optical bistability in semiconductor microcavities, *Phys. Rev. A* **69**, 023809 (2004).
- [10] A. Baas, J.-Ph. Karr, M. Romanelli, A. Bramati, and E. Giacobino, Optical bistability in semiconductor microcavities in the nondegenerate parametric oscillation regime: Analogy with the optical parametric oscillator, *Phys. Rev. B* **70**, 161307 (2004).
- [11] R. Cerna, Y. Léger, T. K. Paraíso, M. Wouters, F. Morier-Genoud, M. T. Portella-Oberli, and B. Deveaud, Ultrafast tristable spin memory of a coherent polariton gas, *Nat. Commun.* **4**, 2008 (2013).
- [12] C. Ouellet-Plamondon, G. Sallen, F. Morier-Genoud, D. Y. Oberli, M. T. Portella-Oberli, and B. Deveaud, Reservoir-induced decoherence of resonantly excited confined polaritons, *Phys. Rev. B* **95**, 085302 (2017).
- [13] S. R. K. Rodriguez, W. Casteels, F. Storme, N. Carlon Zambon, I. Sagnes, L. Le Gratiet, E. Galopin, A. Lemaître, A. Amo, C. Ciuti, and J. Bloch, Probing a Dissipative Phase Transition via Dynamical Optical Hysteresis, *Phys. Rev. Lett.* **118**, 247402 (2017).
- [14] A. Dreismann, H. Ohadi, Y. del Valle-Inclan Redondo, R. Balili, Y. G. Rubo, S. I. Tsintzos, G. Deligeorgis, Z. Hatzopoulos, P. G. Savvidis, and J. J. Baumberg, A sub-femtojoule electrical spin-switch based on optically trapped polariton condensates, *Nat. Mater.* **15**, 1074 (2016).
- [15] D. Bajoni, E. Semenova, A. Lemaître, S. Bouchoule, E. Wertz, P. Senellart, S. Barbay, R. Kuszelewicz, and J. Bloch, Optical Bistability in a GaAs-Based Polariton Diode, *Phys. Rev. Lett.* **101**, 266402 (2008).
- [16] M. Amthor, T. C. H. Liew, C. Metzger, S. Brodbeck, L. Worschech, M. Kamp, I. A. Shelykh, A. V. Kavokin, C. Schneider, and S. Höfling, Optical bistability in electrically driven polariton condensates, *Phys. Rev. B* **91**, 081404 (2015).
- [17] O. Kyriienko, E. A. Ostrovskaya, O. A. Egorov, I. A. Shelykh, and T. C. H. Liew, Bistability in microcavities with incoherent optical or electrical excitation, *Phys. Rev. B* **90**, 125407 (2014).
- [18] A. Askitopoulos, H. Ohadi, A. V. Kavokin, Z. Hatzopoulos, P. G. Savvidis, and P. G. Lagoudakis, Polariton condensation in an optically induced two-dimensional potential, *Phys. Rev. B* **88**, 041308 (2013).
- [19] D. N. Krizhanovskii, K. G. Lagoudakis, M. Wouters, B. Pietka, R. A. Bradley, K. Guda, D. M. Whittaker, M. S. Skolnick, B. Deveaud-Plédran, M. Richard, R. André, and Le Si Dang, Coexisting nonequilibrium condensates with long-range spatial coherence in semiconductor microcavities, *Phys. Rev. B* **80**, 045317 (2009).
- [20] A. Kavokin, P. G. Lagoudakis, G. Malpuech, and J. J. Baumberg, Polarization rotation in parametric scattering of polaritons in semiconductor microcavities, *Phys. Rev. B* **67**, 195321 (2003).
- [21] E. Kammann, T. C. H. Liew, H. Ohadi, P. Cilibrizzi, P. Tsotsis, Z. Hatzopoulos, P. G. Savvidis, A. V. Kavokin, and P. G. Lagoudakis, Nonlinear Optical Spin Hall Effect and Long-Range Spin Transport in Polariton Lasers, *Phys. Rev. Lett.* **109**, 036404 (2012).
- [22] P. Cilibrizzi, H. Sigurdsson, T. C. H. Liew, H. Ohadi, S. Wilkinson, A. Askitopoulos, I. A. Shelykh, and P. G. Lagoudakis, Polariton spin whirls, *Phys. Rev. B* **92**, 155308 (2015).
- [23] A. Askitopoulos, K. Kalinin, T. C. H. Liew, P. Cilibrizzi, Z. Hatzopoulos, P. G. Savvidis, N. G. Berloff, and P. G. Lagoudakis, Nonresonant optical control of a spinor polariton condensate, *Phys. Rev. B* **93**, 205307 (2016).
- [24] See Supplemental Material at <http://link.aps.org/supplemental/10.1103/PhysRevLett.120.225301> for details of the numerical simulations, analogy to the driven damped pendulum and complimentary experimental observations.
- [25] S. H. Strogatz, *Nonlinear Dynamics and Chaos: With Applications to Physics, Biology, Chemistry and Engineering* (Perseus, New York, 2000).
- [26] A. Askitopoulos, T. C. H. Liew, H. Ohadi, Z. Hatzopoulos, P. G. Savvidis, and P. G. Lagoudakis, Robust platform for engineering pure-quantum-state transitions in polariton condensates, *Phys. Rev. B* **92**, 035305 (2015).
- [27] P. Tsotsis, P. S. Eldridge, T. Gao, S. I. Tsintzos, Z. Hatzopoulos, and P. G. Savvidis, Lasing threshold doubling at the crossover from strong to weak coupling regime in GaAs microcavity, *New J. Phys.* **14**, 023060 (2012).
- [28] H. Abbaspour, G. Sallen, S. Trebaol, F. Morier-Genoud, M. T. Portella-Oberli, and B. Deveaud, Effect of a noisy driving field on a bistable polariton system, *Phys. Rev. B* **92**, 165303 (2015).
- [29] For all the measurements here, the ratio of the time interval between successive sweeps,  $T_{\text{Sep}}$ , and the sweep time,  $T_P$ , is kept constant at  $T_{\text{Sep}}/T_P = 5$ .
- [30] W. Casteels, F. Storme, A. Le Boité, and C. Ciuti, Power laws in the dynamic hysteresis of quantum nonlinear photonic resonators, *Phys. Rev. A* **93**, 033824 (2016).